eLIFE elifesciences.org

RESEARCH ARTICLE

Figures and figure supplements

Lateral interactions between protofilaments of the bacterial tubulin homolog FtsZ are essential for cell division

Fenghui Guan *et al*

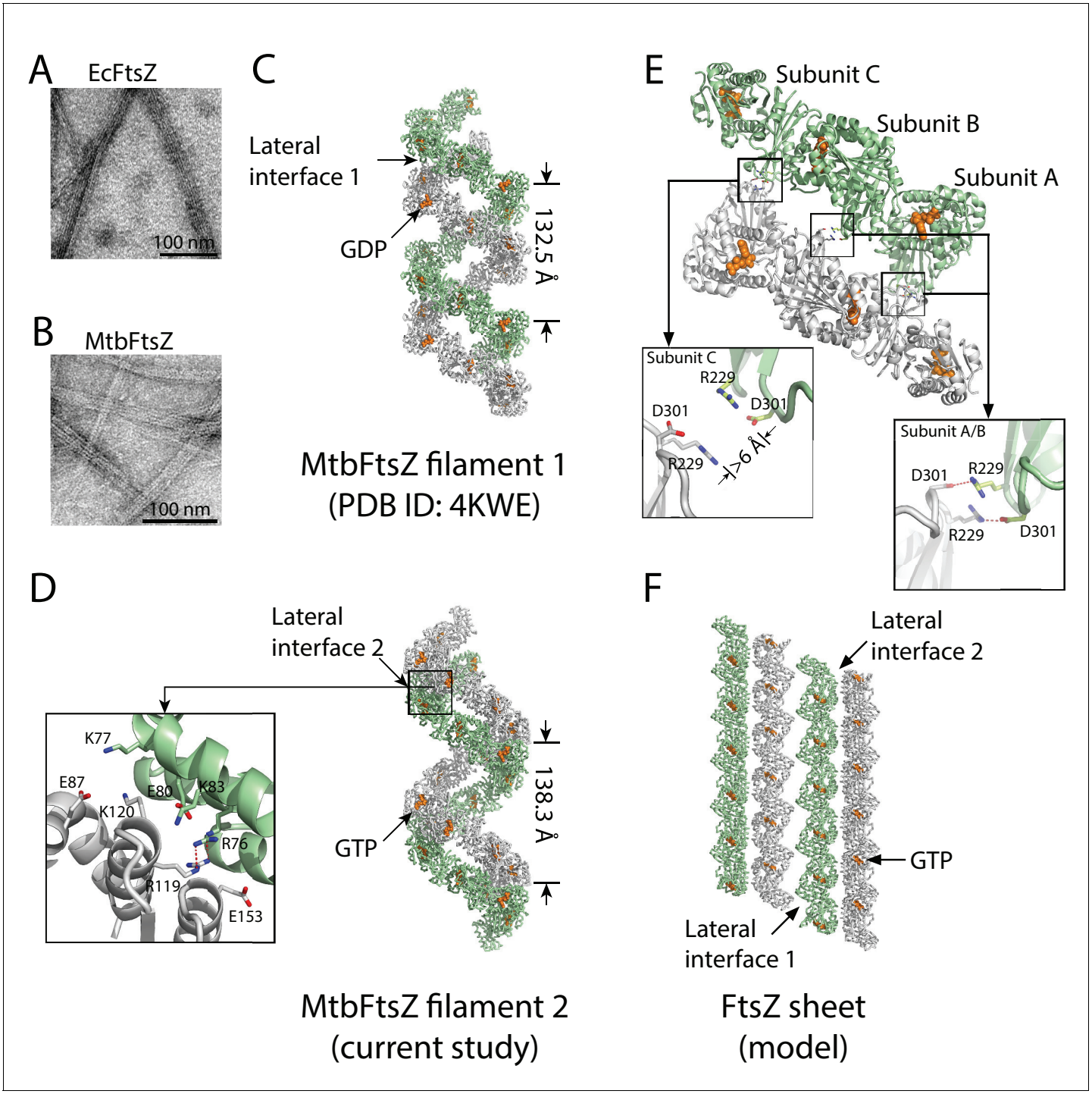

Figure 1. Structures of double-stranded MtbFtsZ-GDP and MtbFtsZ -GTP protofilaments reveal lateral contacts across FtsZ protofilaments. (**A, B**) Electron micrographs of protofilament bundles of EcFtsZ-GTP (**A**) and MtbFtsZ-GTP (**B**). Both were polymerized with the addition of 0.6 mg/mL DEAE-Dextran, and in the presence of 2 mM GTP. (**C, D**) Cartoon representations of double-stranded MtbFtsZ-GDP (**C**; PDB ID: 4KWE) and MtbFtsZ-GTP (**D**; this study) protofilaments containing a total of 24 subunits. The helices have a pitch of 132.5 Å for MtbFtsZ-GDP (**C**) and 138.3 Å for MtbFtsZ-GTP (**D**) protofilaments. Each structure reveals unique lateral interactions across the protofilaments. Inset: atomic details of the lateral interface of the double-stranded MtbFtsZ-GTP protofilaments. (**E**) Molecular details of the lateral interface of the double-stranded MtbFtsZ-GDP protofilaments shown in (**C**). Inset: atomic details of the lateral interactions. (**F**) A structural model for sheet-like bundles of FtsZ protofilaments. Ribbon representation of four straight FtsZ-GTP protofilaments (each containing six subunits, arranged in an antiparallel fashion).

DOI: https://doi.org/10.7554/eLife.35578.003

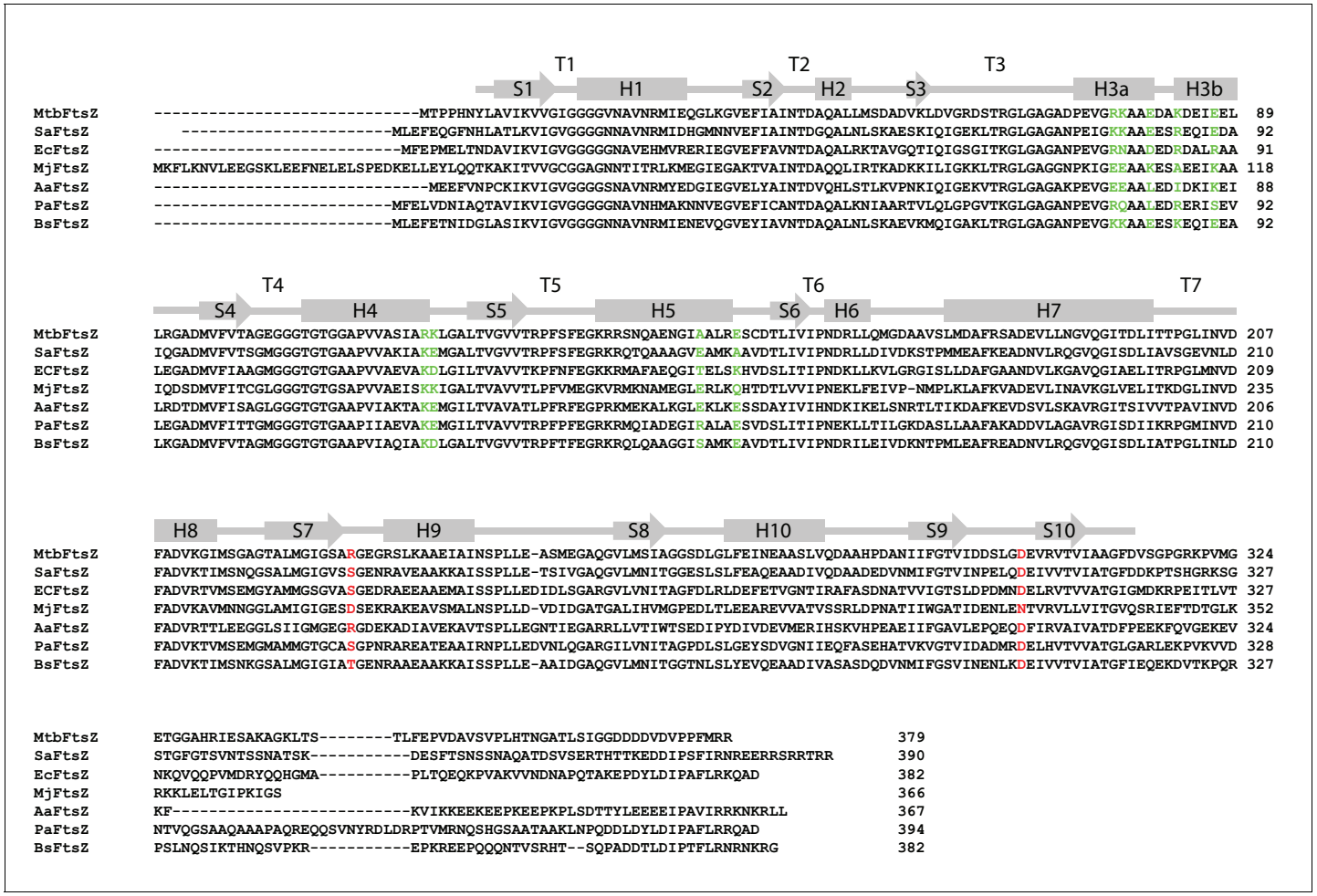

Figure 1—figure supplement 1. Multiple sequence alignment of FtsZ and secondary structure elements. Amino acid sequence alignment of FtsZ from *Mycobacterium tuberculosis* (MtbFtsZ), *Staphylococcus aureus* (SaFtsZ), *Escherichia coli* (EcFtsZ), *Methanococcus jannaschii* (MjFtsZ), *Aquifex aeolicus* (AaFtsZ), *Pseudomonas aeruginosa* (PaFtsZ), and *Bacillus subtilis* (BsFtsZ). The secondary structures of α-helices, *β*-strands, and loops in MtbFtsZ are shown as cylinders, arrows, and lines, respectively. Residues from the observed lateral interfaces in EcFtsZ are highlighted in red (interface 1) and green (interface 2). These residues were subjected to mutagenesis in EcFtsZ in the present study.

DOI: https://doi.org/10.7554/eLife.35578.004

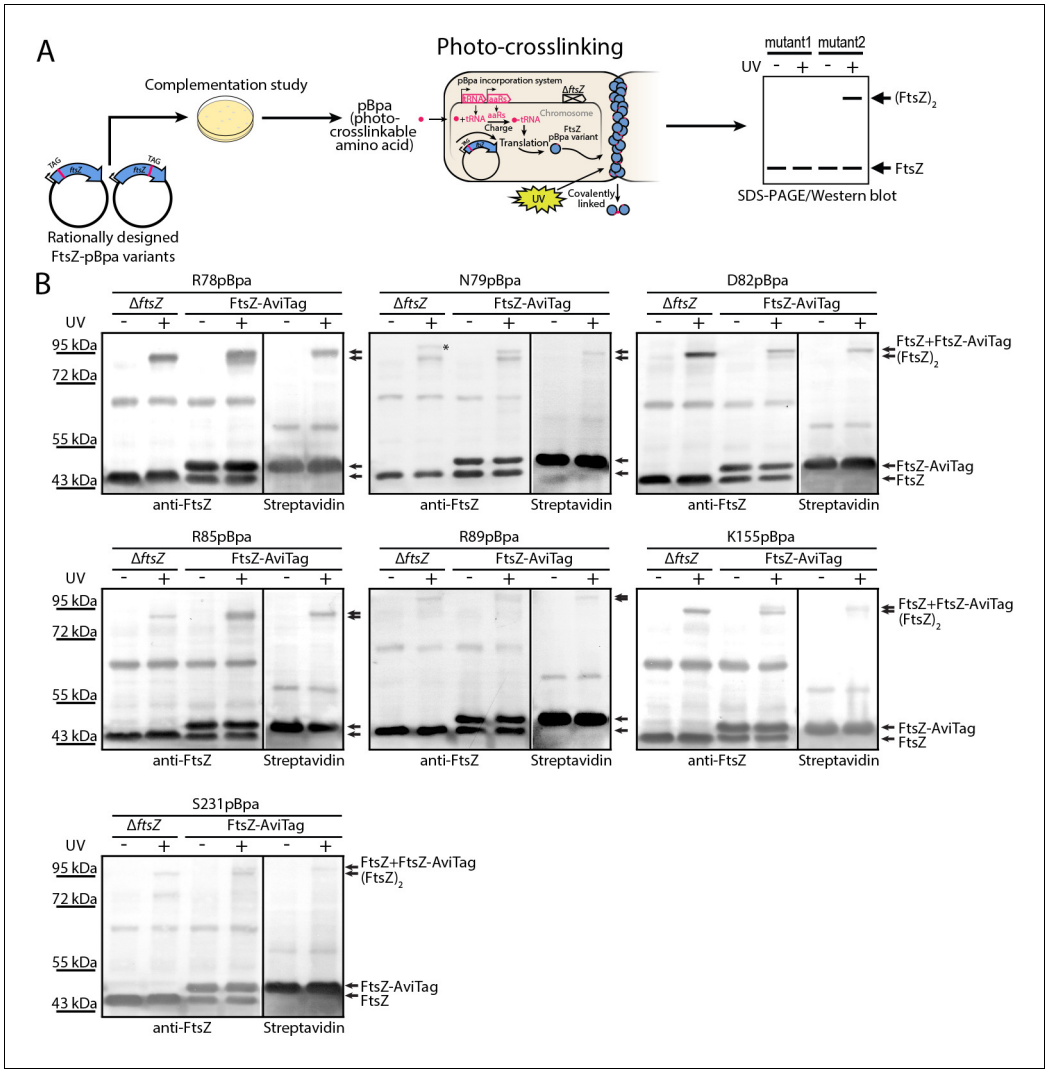

Figure 2. In vivo photocrosslinking characterization of EcFtsZ variants in which pBpa was introduced at specific sites validates inter-protofilament lateral interactions. (**A**) Schematic illustrating the rationale of in vivo photocrosslinking analysis via incorporation of the unnatural amino acid pBpa at specific residue positions of FtsZ. (**B**) Results of blotting analyses of photocrosslinked products with lysates of *E. coli* cells (LY928-*ΔftsZ* or LY928-FtsZ-AviTag) expressing the indicated pBpa variant of FtsZ, using antibodies against EcFtsZ (left) or using alkaline phosphatase-conjugated streptavidin (right). Indicated on the right of each gel are the positions of the non-photocrosslinked monomers and the photocrosslinked dimers of the pBpa variant of FtsZ with or without the AviTag. The asterisk indicates the position of a crosslinked product of FtsZ and another as yet unidentified protein.

DOI: https://doi.org/10.7554/eLife.35578.006

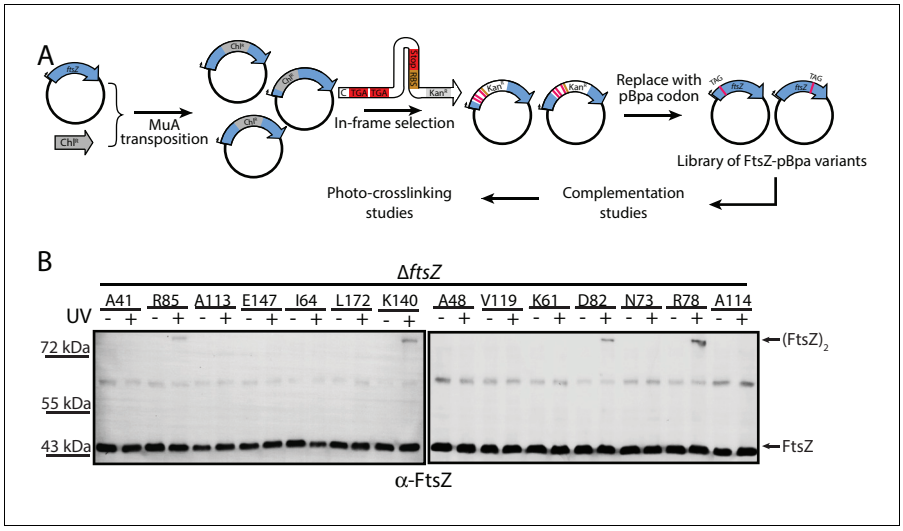

Figure 3. In vivo photocrosslinking characterization of randomly generated EcFtsZ pBpa variants. (**A**) Schematic illustrating the random in vivo photocrosslinking screening strategy for unbiased identification of amino acid positions mediating subunit interactions. (**B**) Immunoblotting analysis of the photocrosslinked products in lysates of *E. coli* LY928-*ΔftsZ* cells that were transformed with the library of plasmids within which the in-frame TAG amber codon was randomly inserted throughout the *ftsZ* gene, as probed with antibodies against EcFtsZ.

DOI: https://doi.org/10.7554/eLife.35578.007

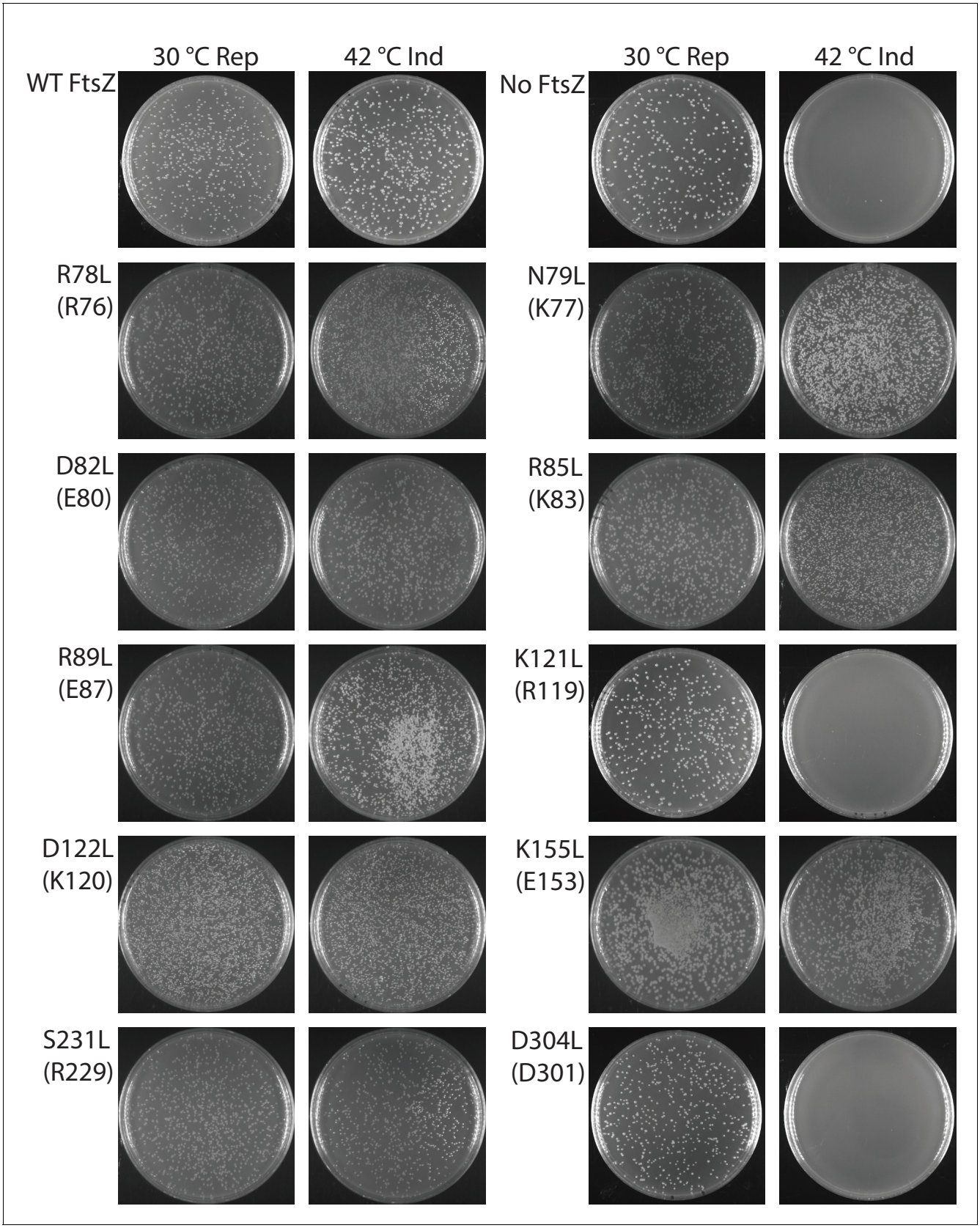

Figure 4. Complementation characterization of EcFtsZ mutants at inter-protofilament lateral interfaces. Ten EcFtsZ mutants were selected based on our crystallographic observations. Mutations were introduced by altering hydrophilic residues to hydrophobic leucine. The division phenotype was

Figure 4 continued on next page

Figure 4 continued

characterized using a *ΔftsZ* strain expressing the EcFtsZ mutants, with conditional expression of wild-type FtsZ from a plasmid at 30°C but not 42°C. 'Rep' and 'Ind' indicate repression and induction media, respectively. For each mutant, the complementation assay was repeated three times.
DOI: https://doi.org/10.7554/eLife.35578.008

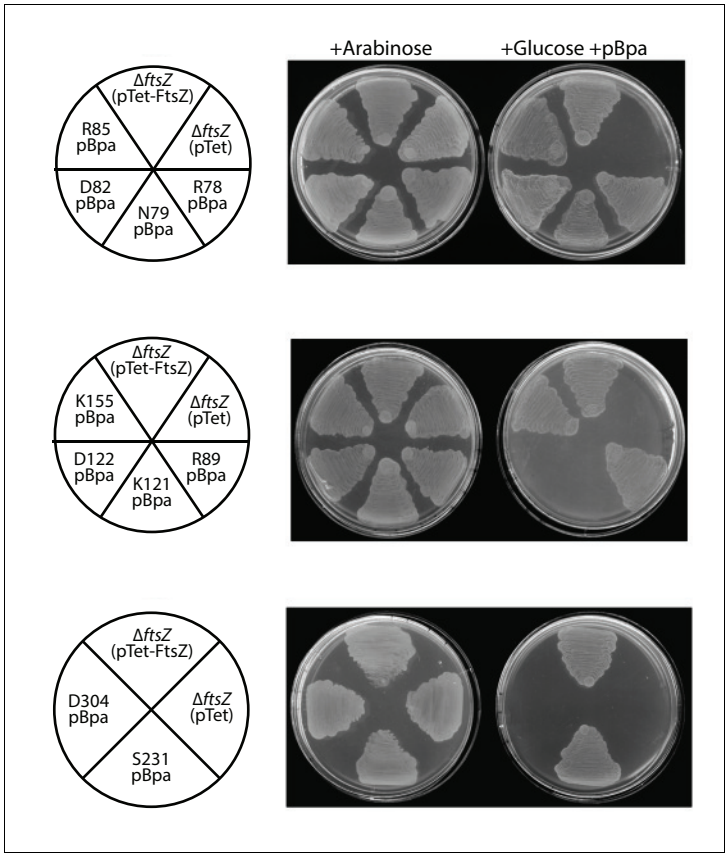

Figure 4—figure supplement 1. Complementation characterization of pBpa-incorporated EcFtsZ variants. Ten replacements of EcFtsZ were selected based on our crystallographic observations. pBpa-incorporated variants were created by altering the corresponding sense codon to an amber TAG stop codon. The FtsZ expression plasmid pTet-FtsZ carrying an in-frame amber mutation was used to transform *E. coli* LY928-Δ*ftsZ* (pJSB100) cells. Cell division, and thus cell growth, could only occur when an FtsZ variant was functional and in the addition of glucose and pBpa.

DOI: https://doi.org/10.7554/eLife.35578.009

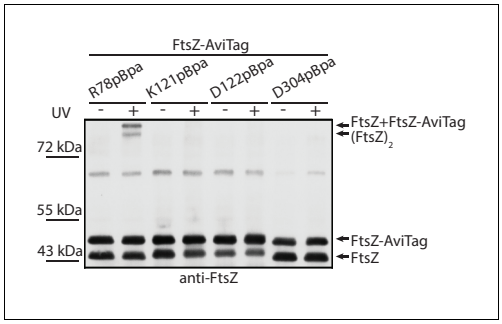

Figure 4—figure supplement 2. Immunoblotting analysis of three pBpa variants of EcFtsZ that failed to complement the *ftsZ* conditional-null strain shows absence of crosslinked dimers. The variants were expressed in LY928-FtsZ-AviTag cells and crosslinked by UV irradiation. Lysate from cells expressing the R78pBpa variant of FtsZ was analyzed as a positive control for photocrosslinked FtsZ dimers.

DOI: https://doi.org/10.7554/eLife.35578.010

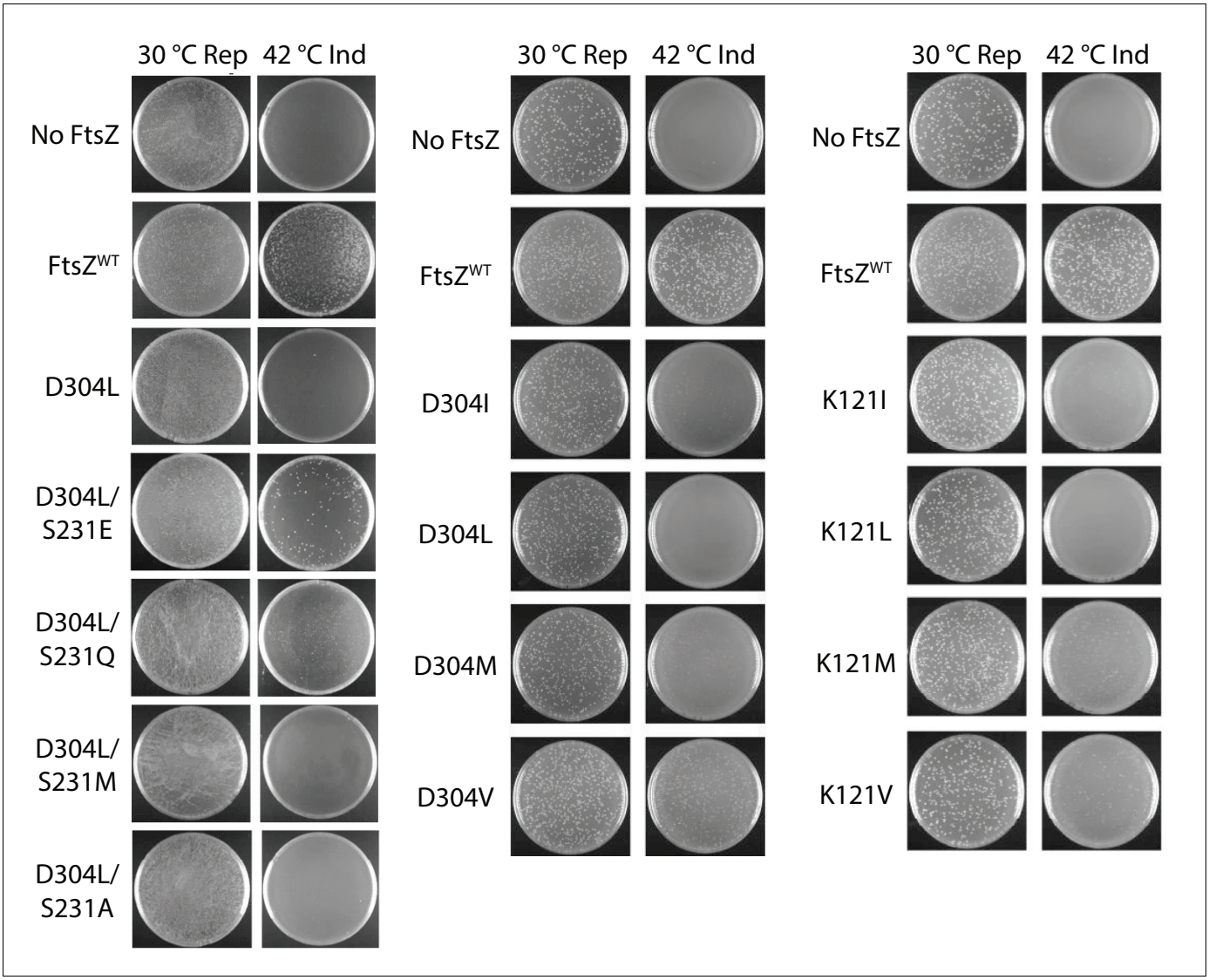

Figure 5. Complementation characterization of EcFtsZ mutants. Mutations were introduced by altering D304 and K121 to different hydrophobic residues. In addition to the D304L mutation, S231 was replaced several other amino acids. The division phenotype was characterized using a *ΔftsZ* strain with expression of the EcFtsZ mutants, and conditional expression of wild-type FtsZ from a plasmid at 30°C but not 42°C. 'Rep' and 'Ind' indicate repression and induction media, respectively. For each mutant, the complementation assay was repeated three times.

DOI: https://doi.org/10.7554/eLife.35578.012

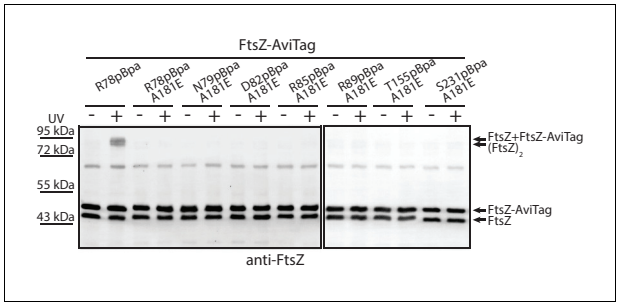

Figure 6. Protofilament formation is required for FtsZ lateral interactions to occur. Streptavidin blotting analyses of photocrosslinked products of EcFtsZ variants in which pBpa was incorporated at the lateral interface in addition to replacement of alanine 181 with glutamate, which is known to disrupt protofilament formation. The R78pBpa variant (with no disrupting replacement at position 181) was analyzed as a positive control.

DOI: https://doi.org/10.7554/eLife.35578.013

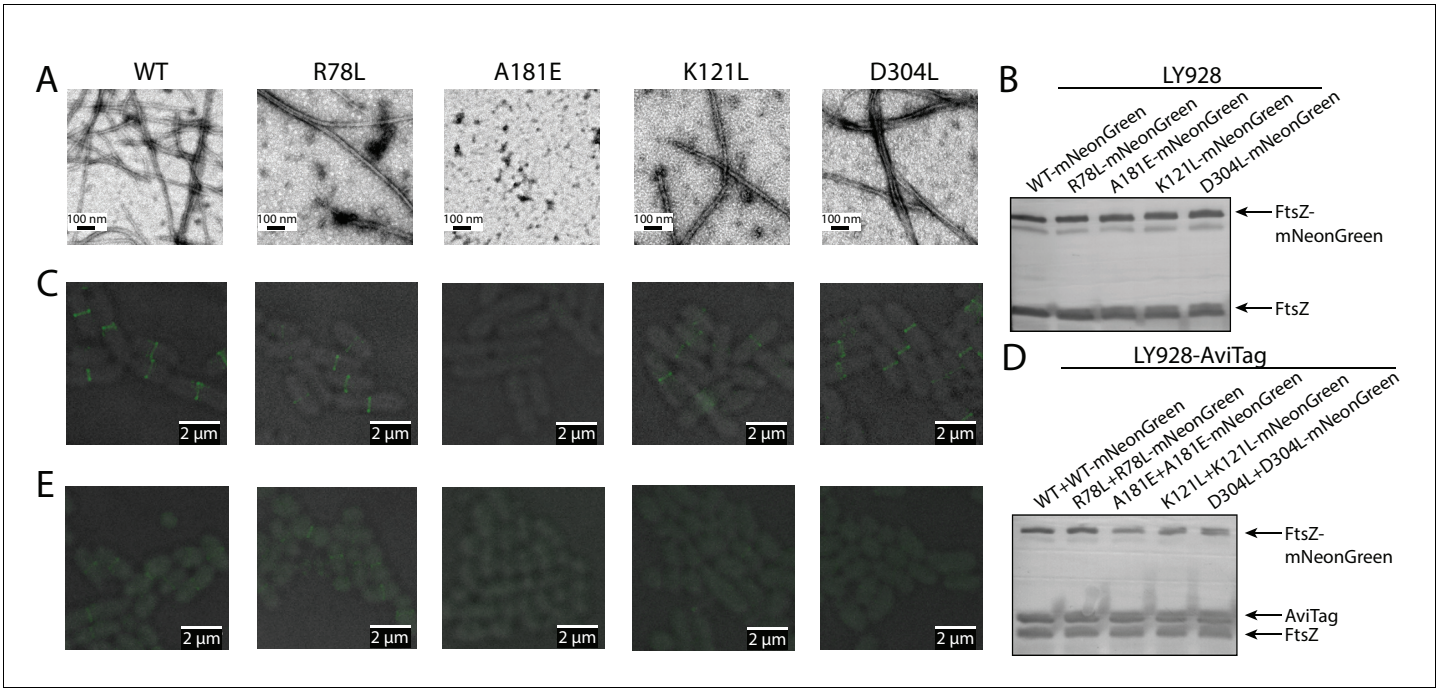

Figure 7. Disruption of the integration of lateral interaction-impaired protofilaments into the Z-ring. (**A**) Electron microscopy analysis of GTP-dependent polymerization (with the addition of 0.6 mg/ml DEAE-Dextran) of wild-type or mutated EcFtsZ in which all mutants except A181E form protofilaments similar to wild-type. (**B**) Western blot analysis of levels of mNeonGreen fusions to wild-type EcFtsZ and mutants. The cellular proportions of mutant FtsZ were ~40%. (**C**) Fluorescence microscopy demonstrates that low-level expression of laterally disruptive EcFtsZ mutants fused to mNeonGreen does not affect protofilament integration into the Z-ring. (**D**) Western blot analysis of levels of mNeonGreen fusions to wild-type EcFtsZ and mutants, as well as the AviTagged version. The cellular proportions of mutant FtsZ (mNeonGreen-tagged and untagged) were ~60%. (**E**) Dominant expression of disruptive EcFtsZ mutants fused to mNeonGreen hinders protofilament integration into the Z-ring, unlike wild-type or the non-disruptive interfacial mutant EcFtsZ^{R78L}.

DOI: https://doi.org/10.7554/eLife.35578.014

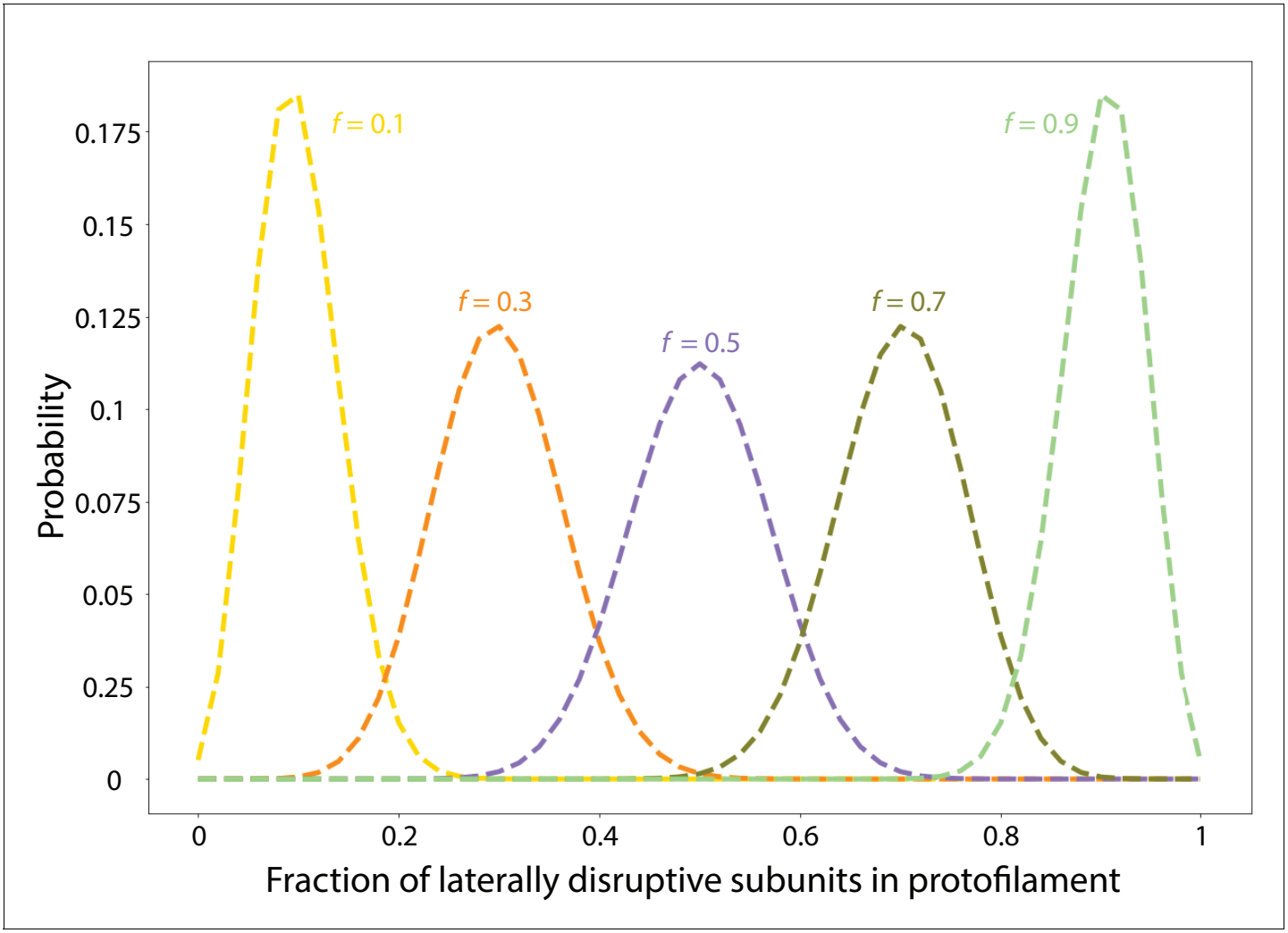

Figure 7—figure supplement 1. Laterally disruptive FtsZ subunits incorporate into FtsZ protofilaments following a binomial distribution. Shown are the results of a model in which we assume that all FtsZ protofilaments are 50 subunits long and compute the fraction *X* of each protofilament that is composed of laterally disruptive subunits, as a function of the overall proportion *f* of laterally disruptive subunits in a cell. The probability density function is the Binomial distribution $P(X = k) = 50kf^k(1-f)^{50-k}$.

DOI: https://doi.org/10.7554/eLife.35578.015

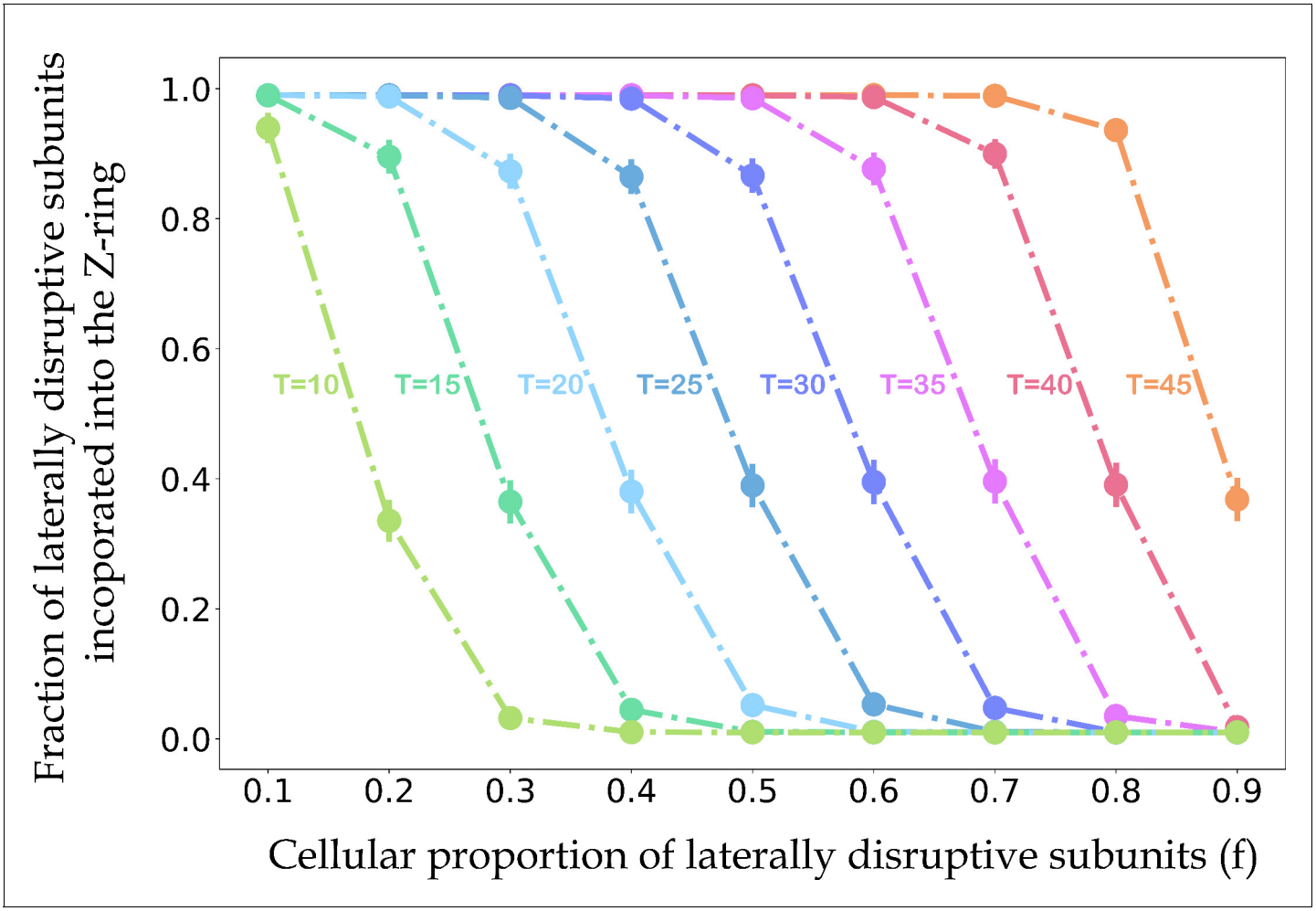

Figure 7—figure supplement 2. The relationships between the fraction of laterally disruptive subunits incorporated into the Z-ring, the cellular proportion of disruptive subunits, and the maximum number of disruptive subunits that still allow for efficient Z-ring lateral association. For each value of the cellular proportion of disruptive subunits (*f*) and threshold for efficient Z-ring incorporation (T), we performed 10,000 independent simulations. In each simulation, we generated a vector $\mathbf{X} = (x_1, x_2, \ldots, x_{200})$, where x_i represents the number of laterally disruptive subunits in the i^{th} protofilament, selected from the Binomial distribution with mean 50*f* (***Figure 7—figure supplement 1***). For a protofilament with more or less laterally disruptive subunits than the threshold *T*, we set the probability of Z-ring incorporation to 0.01 or 0.99, respectively. The Boolean vector **V** represents the incorporation state of each protofilament. We then calculated the percentage of laterally disruptive subunits incorporated into the Z-ring as $\frac{\mathbf{X}\cdot\mathbf{V}}{\sum_{i=1}^{200} x_i}$. Circles indicate the mean percentages of laterally disruptive subunits in the Z-ring across simulations with a given value of *f* and *T*, and solid vertical lines represent the standard deviations. As the total proportion of laterally disruptive subunits increases, the proportion of laterally disruptive subunits incorporated into the Z-ring decreases, consistent with our experimental results showing a faint or non-existent Z-ring with dominant expression of laterally disruptive mutants (***Figure 7E***).

DOI: https://doi.org/10.7554/eLife.35578.016